Infrared Physics & Technology 92 (2018) 13–17

Contents lists available at ScienceDirect

Infrared Physics & Technology

journal homepage: www.elsevier.com/locate/infrared

Regular article

Ge-based mid-infrared blocked-impurity-band photodetectors ☆

Jiaqi Zhu [a], He Zhu [b,*], Hanlun Xu [a], Zeping Weng [a], Huizhen Wu [a,*]

[a] Department of Physics and State Key Laboratory of Silicon Materials, Zhejiang University, Hangzhou, Zhejiang 310027, PR China
[b] College of Electronics and Information, Hangzhou Dianzi University, Hangzhou, Zhejiang 310018, PR China

HIGHLIGHTS

- RBM has a lower optimum bias but a larger maximum of photocurrent.
- The finding above is caused by the slope of the electric field profile in BL.
- The longer BL is, the larger photocurrent under RBM is.
- There is a red-shift for photocurrent spectrum of RBM compared with that of FBM.
- Lengthening BL is expected to improve performance of BIB detectors under RBM.

ARTICLE INFO

Article history:
Received 8 January 2018
Revised 11 March 2018
Accepted 28 April 2018
Available online 5 May 2018

Keywords:
Blocked impurity band detector
Mid-infrared
Operation modes
Blocking layer length

ABSTRACT

Mid-infrared blocked-impurity-band (BIB) photonic detectors are developed by sulfur (S) ions implantation into germanium (Ge) crystal. The detectors demonstrate wide photoresponse spectra ranging from 2 to 10 μm with peak response at about 6 μm. We characterize photocurrent spectra of two operating modes, forward bias mode (FBM) and reverse bias mode (RBM), and find that RBM has a lower optimum bias but a bigger photocurrent. Effect of different blocking layer (BL) length on photocurrents for the two operating modes is studied. When BL length increases, the ratio of the relative photocurrent under RBM to that under FBM at respective optimum bias enlarges. The slope of the electric field profile in BL leads to the differences of optimum bias and maximum photocurrent between two modes. The electric field strength in AL under RBM strengthens as BL length increases, resulting in larger photocurrent for longer BL.

1. Introduction

Mid-infrared (MIR), in the wavelength range of 3–5 μm, is intensely desirable for varied applications in pollution monitoring, optical gas sensors, thermal imaging, chemical analysis, and spatial orientation, while various MIR detectors have been developed for practical applications in these fields [1–4]. At present, there are mainly three types of material systems pursued to realize high-sensitivity MIR photonic detectors. Low-bandgap materials, such as HgCdTe [5,6], are preferred due to their high responsivity and detectivity (D^*). However, there remain problems in the epitaxial growth of HgCdTe-based materials because of the presence of fearful interface instabilities and void-defect densities, which can be seen in the high uncertainty and fluctuation of the value of D^* [7]. Type Ⅱ strained-layer superlattices with materials such as InAsSb/InSb or InGaSb/InAs have been widely studied [8,9]. But the epitaxial-growth technique for the antimonides is not mature and reliable enough for group V intermixing during growth, either. Moreover, surface passivation is also a big concern for antimonide-based devices. Intersubband transitions in quantum-confined heterostructures in III-V compounds can be used for MIR detection as well [10–12]. Nevertheless, the selection rules of the intersubband transitions prevent normal-incidence photons from being absorbed by transitions from the ground state to the excited states [11], and because of the short lifetime of electrons in the excited state (~5 ps), the electrons largely relax back to the ground state before they can escape from the quantum well and contribute to the photocurrent [13].

The blocked-impurity-band (BIB) detector structure, presented in 1986 by Petroff and Stapelbroek [14], has a good chance to be employed in MIR photonic detection to overcome the shortcomings mentioned above. In this detector system, the active layer is doped so heavily that the absorption efficiency gets increased

☆ This work was supported by Natural Science Foundation of China under Grant 61290305 and Grant 11374259.
* Corresponding authors.
E-mail addresses: hezhu@hdu.edu.cn (H. Zhu), hzwu@zju.edu.cn (H. Wu).

https://doi.org/10.1016/j.infrared.2018.04.015
1350-4495/

and hopping conduction gets realized in the impurity band, while the dark current through the device is still effectively suppressed by skillfully employing an ultrapure blocking layer (BL) to block the impurity band conduction. Consequently, the working temperature of the device can be improved greatly. What's more, the technologies applied in fabricating BIB detectors are easily implemented, especially for ion-implantation BIB detectors whose absorbing layer (AL) is achieved by ion implantation [15]. In forward bias operation, n-type BIB detectors are biased with a positive voltage on the contact near the BL [16]. Photo-generated carriers are collected from depletion region, where a linearly decreasing electric field extends from the BL/AL interface into the AL, and transported through the BL to the front contact [17].

It has been already a common way to achieve far-infrared (especially terahertz) detection that germanium (Ge) is doped with specific impurity atoms. The response of Ga-doped Ge photoconductor can obtain a cutoff wavelength of about 113 μm [18]. It even reaches about 200 μm by means of doping B into Ge [15]. In this paper, we fabricated MIR BIB detectors where the AL is developed by implanting sulfur (S) ions into high purity host Ge (Ge:S). The response spectra of this detectors ranges from 2 to 10 μm with peak response at about 6 μm. The influence of two operating modes, forward bias mode (FBM) and reverse bias mode (RBM, where the electrode contacting the BL is negatively biased), on the photoresponse of detectors with different BL length is studied in detail. It is found that there exists a lower optimum bias but a larger maximum of photocurrent for RBM. Moreover, there is a red-shift for photocurrent spectrum of RBM compared with that of FBM. We also find that the ratio of the relative photocurrent under RBM to that under FBM at respective optimum bias increases with BL length. In order to understand these phenomena deeply, electric field distributions are calculated in view of doping concentration in BL.

2. Experimental procedures

As shown in Fig. 1(a), the device structure is interdigital, one cell of which consists of a S-doped AL (1 μm in thickness and $20 \times 400\ \mu m^2$ in area), an intrinsic BL (as well as the high purity Ge substrate), two heavily phosphor-doped contact layers (CL, 1 μm in thickness) and two aluminum-deposited contacts. There are three kinds of BL length, 5 μm, 7 μm and 9 μm, in different interdigital structures. The AL and the CL are both developed by ion implantation technology.

We began the fabricating process with depositing a 200 nm SiO_2 layer on the substrate by plasma enhanced chemical vapor deposition (PECVD), which serves as insulating layer and alignment mark in the following process. Before ion implantation, the other regions of Ge wafer were covered by corresponding photoresist pattern (about 3 μm in thickness) as protector. In order to obtain homogenous AL, an implanting scheme including several different-energy and different-concentration steps was used. The final concentration of about $2 \times 10^{17}\ cm^{-3}$ was obtained, which was verified by Hall Effect characterization. In view of the channeling effect, moreover, S ion beam is incident 7° off the substrate ⟨1 0 0⟩ axis, so is P ion beam when ion implanting in the later process. After removing the photoresist, the same processing steps were adopted to developing CL by implanting P ions with higher concentration (up to $1 \times 10^{20}\ cm^{-3}$) than S ions to merge the impurity level into the conduction band. The following is rapid thermal annealing (RTA) technique (800, 30 s) for electrically activating the dopant (S and P) atoms and repairing the damage caused by implantation as well. Subsequently, a second 200 nm SiO_2 layer is deposited on the surface by the same method serving as passivation layer to suppress the surface recombination rate. After opening the contact region, an 1 μm Al film was deposited by magnetron sputtering, followed by 300 °C annealing for 30 min to form ohmic contact with the CL. Fig. 1(b) shows the scanning electron microscope (SEM) image of the fabricated BIB detectors.

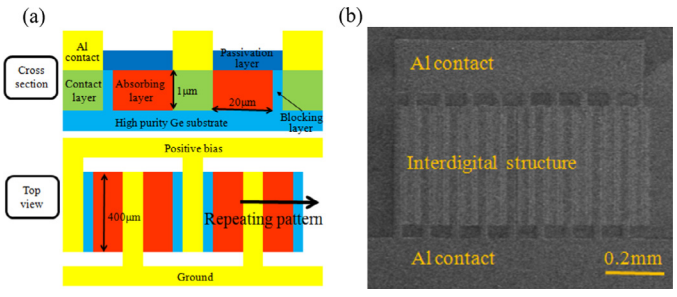

Fig. 1. (a) Cross section and top view (without passivation layer) of the Ge:S BIB detector. (b) A SEM image of the fabricated Ge:S BIB detector.

The packaged detectors were mounted in a closed cycle refrigeration dewar. The photocurrent spectra were measured with a VERTEX 80/80v Fourier-transform infrared spectrometer. Without specific statement there-in-after, the photoresponse characterizations of the detectors were performed at 4 K.

3. Results and discussion

Fig. 2(a & b), (d & e) and (g & h) show relative photocurrent spectra of Ge:S detectors with different BL length at various bias voltages under RBM or FBM. All the spectra are cutoff at approximate 10 μm (124 meV) which is smaller than the donor ionization energy (180 meV) of S impurity atoms in Ge. This phenomenon indicates the formation of the impurity band and narrowing of Ge band gap. By the way, for the device with BL length of 5 μm, the responsivity is 0.4 A/W and the detectivity is 9.7×10^{10} cm $Hz^{1/2}/W$ at 1.0 V under FBM at 4 K. Moreover, there is an optimum bias in each photocurrent spectrum where the photocurrent reaches maximum. The optimum bias can be clearly seen for the two modes in Fig. 2(c & f & i), which show the maximum photocurrent in the spectra vs bias voltage for the two modes of 5 μm, 7 μm and 9 μm, respectively. Let's take the detector with BL length of 5 μm for example, besides, the bias applied is negative, that is, the detector works under RBM. When the bias is lower than 1.0 V, the photocurrent increases with the bias. However, it decreases as the bias rises beyond 1.0 V. With different BL length or different operating mode, the optimum bias is evidently different. Table 1 lists the relation between the optimum bias and BL length as well as operating mode. We can see that the optimum bias increases with BL length under each operating mode. Furthermore, no matter what BL length is, the optimum bias of RBM is lower than that of FBM.

The comparison of the photocurrent spectra of the detectors with different BL length under RBM and FBM at respective optimum bias is shown in Fig. 3(a)–(c), and corresponding statistic of the relative photocurrent ratio is given in Table 1, where R_R and R_F represent the photocurrent of RBM and FBM, respectively. It is obvious that the photocurrent under RBM is much larger than that under FBM for all detectors. Interestingly, the ratio of the photocurrent under RBM to that under FBM at respective optimum bias increases with BL length. What is also interesting is that, the relative photocurrent spectrum under RBM shows a small red-shift compared with that under FBM for all detectors, as shown in Fig. 3. The shifts at 50% of the maximum photocurrent for BL of 5 μm, 7 μm and 9 μm, are 0.22 μm, 0.15 μm and 0.18 μm, respectively.

Fig. 4(a) and (b) display the energy band diagram for the detector under FBM and RBM, respectively. When the test temperature is low enough, almost all electrons are assumed to be frozen out